Eur. Phys. J. B **39**, 417–425 (2004)
DOI: 10.1140/epjb/e2004-00212-0

THE EUROPEAN PHYSICAL JOURNAL B

Mössbauer, X-ray diffraction and AC susceptibility studies on nanoparticles of zinc substituted magnesium ferrite

B.K. Nath[1], P.K. Chakrabarti[2], S. Das[3,a], Uday Kumar[4], P.K. Mukhopadhyay[4], and D. Das[1,b]

[1] Inter University Consortium for DAE facilities, 3/LB8, Bidhannagar, Kolkata 700 098, India
[2] Physics Department, Asutosh College, Kolkata 700 026, India
[3] Central Glass and Ceramic Research Institute, Kolkata 700 032, India
[4] LCMP, S.N. Bose National Centre for Basic Sciences, 3/JD, Bidhannagar, Kolkata 700 098, India

Received 6 August 2003 / Received in final form 16 April 2004
Published online 23 July 2004 –

Abstract. Nanoparticles of zinc substituted Mg-ferrite with compositions $Mg_{(1-x)}Zn_xFe_2O_4$ ($x = 0.15, 0.30$ and 0.50) having particle sizes in the range 6.4 nm to 21.4 nm prepared by the co-precipitation method were characterized by ^{57}Fe Mössbauer spectroscopy, X–ray diffratometry and AC magnetic susceptibility measurements. Mössbauer measurements at room temperature and down to 20 K clearly indicate presence of superparamagnetic particles in all the samples. AC magnetic susceptibility data show lowering of blocking temperature with decrease of particle size. Superparamagnetic relaxation was observed for larger particle size in samples with higher Zn content, which is attributed to the weakening of A-B exchange interaction in ferrite lattice due to replacement of Fe^{3+} in tetrahedral site by Zn^{2+} ions.

PACS. 75.50.Tt Fine-particle systems; nanocrystalline materials – 76.80.+y Mössbauer effect; other gamma-ray spectroscopy – 75.30.Cr Saturation moments and magnetic susceptibilities

1 Introduction

Recently nano-particles of magnetic materials have been widely studied because of their novel electric, magnetic and optical properties, which are considerably different from those of their bulk counterparts [1–3]. These systems have potential applications in various fields of modern technologies viz., magnetic resonance imaging contrast agents, data-lifetime in high-density information storage, ferrofluid technology and magneto caloric refrigeration [4–7]. Superparamagnetism is a unique feature of magnetic nano-particle systems. Ultra-fine nano-particles of these materials exhibit interesting phase transition from superparamagnetic (SPM) to ferri/ferro magnetic state or vice versa with variation of temperature depending on their sizes. The major factors that control superparamagnetism are magnetic anisotropy and the volume of the nano-particles. The factors that are responsible for magnetic anisotropy are electron spin-orbital angular momentum coupling at lattice sites in crystals, dipole-dipole interaction among the magnetic ions, shape of nanoparticles etc. The strength of the spin-orbital angular momentum coupling depends mainly on the value of magnetic moment of the atoms involved in the coupling, their relative distances and symmetry of the lattice site. These factors can be systematically varied in case of metal oxides, particularly in case of mixed spinel ferrites [8,9]. Consequently, the onset of superparamagnetism of these classes of materials may be achieved at a desired temperature by controlling the above parameters. In Mg-ferrite, the Mg^{2+} ions are diamagnetic and therefore the magnetic coupling originates from Fe^{3+} cations only. Hence the strength of the coupling may be relatively weaker than those of other ferrites where both divalent and trivalent cations have large magnetic moments. This weaker coupling reduces the anisotropy energy of the system, which facilitates the onset of SPM relaxation in bigger size particles even at room temperature. Chen et al. [10] have reported SPM behaviour of nanocrystalline Mg-ferrite for 7.6 nm and 13 nm particles. They have also reported that Mg cations occupy 40% of the tetrahedral sites and 30% of the octahedral sites. Again, the degree of inversion in magnesium ferrite may be further altered by substitution of zinc ferrite, as zinc cations have a strong tendency to occupy tetrahedral sites replacing Fe^{3+} ions, which eventually go to octahedral sites. Being a diamagnetic cation, Zn^{2+} in tetrahedral sites may further reduce the magnetic couplings as the strength of A-B exchange interaction decreases with increase of Zn substitution. Thus, mixed spinel ferrite $Mg_{(1-x)}Zn_xFe_2O_4$ may be ideally suited for

[a] *Present address*: Department of Physics, Jadavpur University, Kolkata - 700032, India
[b] e-mail: ddas@alpha.iuc.res.in

the study of SPM relaxation for bigger particle sizes at room temperature.

In this paper, we report the preparation and characterization of nanocrystalline $Mg_{(1-x)}Zn_xFe_2O_4$ ($x = 0.15$, 0.30, and 0.50) mixed spinnel ferrites prepared by the co-precipitation method. The as-prepared samples were heat treated at different temperatures to yield different sizes of nano-particles. All these samples were characterized by X-ray diffractometry. Mössbauer spectra have been recorded from room temperature (RT) down to 20 K. AC magnetic susceptibility measurements were carried out in the temperature range from 400 K to 80 K. The SPM relaxation in the present case has been observed at room temperature for 21.4 nm particles with 50% Zn substitution.

2 Experimental

The samples of $Mg_{(1-x)}Zn_xFe_2O_4$ ($x = 0.15$, 0.30, and 0.50) were prepared by the standard co-precipitation method. Anhydrous ferric chloride ($FeCl_3$), magnesium chloride ($MgCl_2 \cdot 6H_2O$) and zinc sulphate ($ZnSO_4 \cdot 7H_2O$) were used as starting materials and a complete homogeneous solution of these salts were prepared by dissolving the salts in deionised water. A few drops of concentrated hydrochloric acid were added to obtain a clear solution. The composition ratios of Fe:Mg:Zn were taken as $2 : (1 - x) : x$. The solution was then heated to about 80 °C. NaOH solution (0.4 M/l) was taken in a conical flux and was heated with vigorous magnetic stirring. The hot solution of the salts was quickly transferred to the alkali medium for fast reaction and the final pH of the solution was maintained at 11. The stirring was continued for about two hours at about 80 °C for complete digestion. To obtain a neutral pH condition, the co-precipitated particles were washed several times and finally filtered and dried at 100 °C for 12 h. The dried samples were annealed at various temperatures to obtain the desired mixed ferrite of different sizes.

X-ray diffraction (XRD) patterns were taken in an Xpert Pro Phillips X-ray diffraction unit with Cu K_α radiation ($\lambda = 0.15425$ nm). Mössbauer measurements were carried out using a PC based spectrometer having 1024 channels MCA card operating in constant acceleration mode. All measurements were done in transmission geometry using a 10 mCi ^{57}Co source in Rh matrix. The spectrometer was calibrated with a 12 μm thick high purity natural iron foil. Low temperature measurements were carried out by mounting the sample in the cold head of a closed cycle refrigerator (model CCS 850) supplied by Janis Research Inc. with a special anti-vibration stand. No line broadening could be detected due to expander vibration. The temperature of the sample was controlled with an accuracy of ±0.1 K using a temperature controller (Lake Shore). AC magnetic susceptibility measurements were carried out in a standard double coil arrangement. Measuring frequency and magnetic field were about 33 Hz and 100 Oe respectively. The samples were taken in pellet form of about 8 mm diameter prepared by pressing the powder at pressure of about 12 MPa. Measurements were carried out in the temperature range 80–400 K in a liquid nitrogen cryostat. The temperature was measured by a calibrated platinum resistance thermometer.

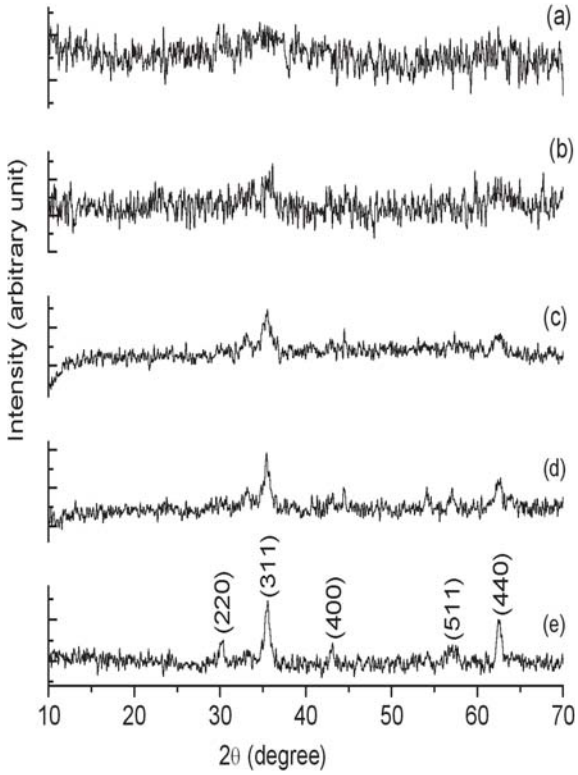

Fig. 1. X-ray diffraction patterns of $Mg_{0.85}Zn_{0.15}Fe_2O_4$ samples annealed at (a) 300 °C (b) 400 °C (c) 500 °C (d) 600 °C (e) 720 °C.

3 Results and discussion

3.1 X-ray diffraction analysis

The as prepared samples were annealed in the temperature range 300 °C to 720 °C to get particles of different sizes. XRD patterns of all the heat-treated samples having different Zn contents are shown in Figures 1, 2 and 3. It is evident from the XRD patterns of $Mg_{0.85}Zn_{0.15}Fe_2O_4$ annealed at 300 °C and 400 °C respectively (Figs. 1a and 1b) that for this sample, the ferrite phase did not form even after heating the precipitate at 400 °C for 12 h. Also, AC magnetic susceptibility measurements of these samples ($Mg_{0.85}Zn_{0.15}Fe_2O_4$ annealed at 300 °C and 400 °C) did not give any magnetic contribution, which confirms the presence of non-magnetic amorphous phase. For the samples with Zn substitution 0.30 and 0.50, a spinel ferrite phase has formed on heat treatment of the precipitate for 12 h at 300 °C (Figs. 2a and 3a) which indicates that increase of Zn content in Mg-ferrite facilitates the formation of nanocrystalline spinel phase even at a low sintering temperature.

Lattice parameters of all the heat-treated samples were evaluated from the identified peaks (as marked in all XRD

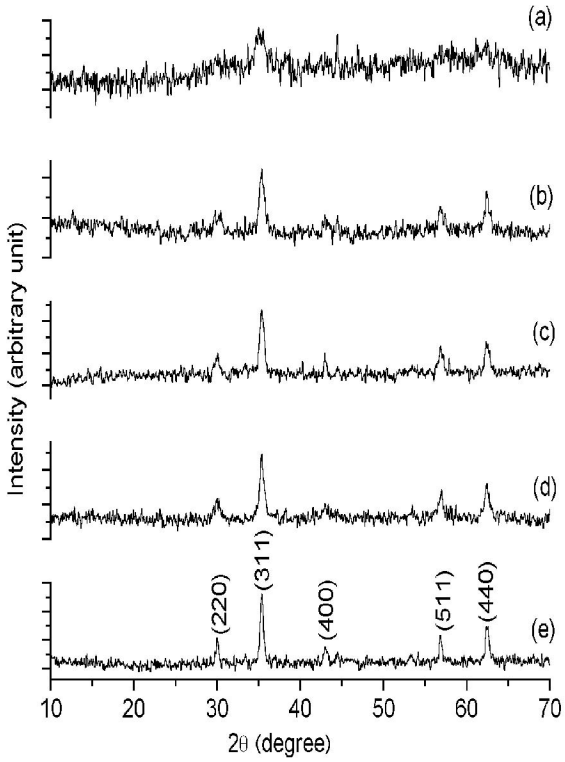

Fig. 2. X-ray diffraction patterns of $Mg_{0.70}Zn_{0.30}Fe_2O_4$ samples annealed at (a) 300 °C (b) 400 °C (c) 500 °C (d) 600 °C (e) 720 °C.

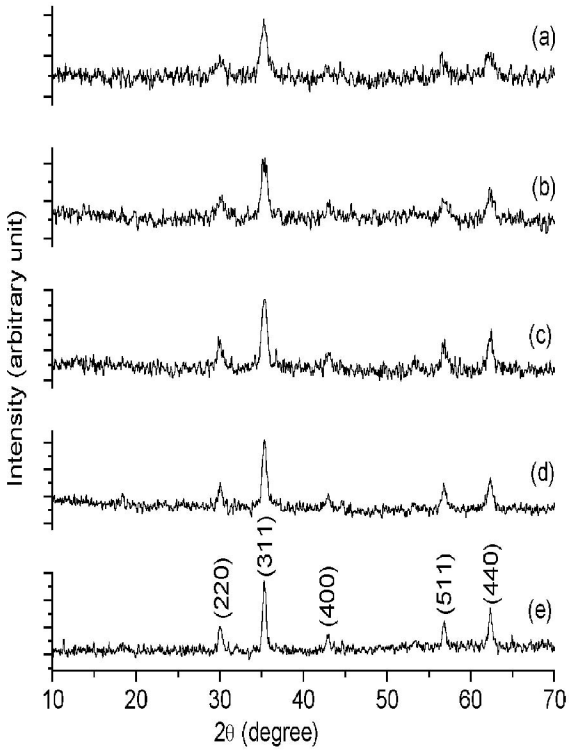

Fig. 3. X-ray diffraction patterns of $Mg_{0.50}Zn_{0.50}Fe_2O_4$ samples annealed at (a) 300 °C (b) 400 °C (c) 500 °C (d) 600 °C (e) 720 °C.

Table 1. Heat treatment schedules, lattice parameters, average particle sizes and blocking temperatures.

Sample Composition	Annealing Temperature (°C)	Lattice Parameter a (nm)§	Average particle size ¶ (nm)	Blocking temperature T_B^*(K)
$Mg_{0.85}Zn_{0.15}Fe_2O_4$	500	0.8414	8.3	246
	600	0.8409	11.2	260
	720	0.8396	12.0	277
$Mg_{0.70}Zn_{0.30}Fe_2O_4$	300	0.8492	6.4	105
	400	0.8421	11.4	230
	500	0.8419	12.3	257
	600	0.8417	14.0	321
	720	0.8419	20.5	362
$Mg_{0.50}Zn_{0.50}Fe_2O_4$	300	0.8440	10.4	105
	400	0.8431	11.2	128
	500	0.8425	13.4	174
	600	0.8422	15.9	194
	720	0.8428	21.4	271

§ maximum error ±0.0004 nm; ¶ maximum error ±1 nm; * measured from maxima of χ'–T curves.

figures) and the corresponding values are tabulated in Table 1. These lattice parameter values confirm the formation of mixed spinel Mg-Zn-ferrite. No peaks corresponding to additional crystalline components were detected in the spinel nano-ferrites.

The average particle sizes of all the heat treated samples were determined from the line broadening of the (311) peaks using Scherrer equation $D = k\lambda/(\beta\cos\theta)$, where D is the average particle size, k is a shape function for which a value of 0.9 is used and λ is the wavelength of the incident X-ray. Here $\beta = \sqrt{(\beta_0^2 - b_0^2)}$, where β_0 is the full width at half maximum (FWHM) of the (311) peak and b_0 is the same for large crystallites. The value of β_0 was obtained from the fitting of the (311) peak to Lorentzian function. The uncertainties in particle size

determination were estimated from the errors in the fitting procedures which lie in the range ±1 nm. The average particle sizes of all the heat-treated samples are in the range 6.4 nm to 21.4 nm and are presented in Table 1.

3.2 Mössbauer analysis

Mössbauer spectroscopy is a powerful technique to characterize magnetic nano particles undergoing SPM relaxation. For extremely small particles with uniaxial anisotropy, the energy barrier, which separates the two easy directions of magnetization, may be smaller than the thermal energy even at room temperature. This leads to spontaneous fluctuation of the magnetization direction having relaxation time given by [11]

$$\tau = \tau_0 \exp(KV/k_B T) \quad (1)$$

where τ_0 (10^{-9}–10^{-10} s) is the inverse of the natural frequency of the gyromagnetic precession, K is the anisotropy energy constant, V is the volume of the particle, k_B is the Boltzmann constant and T is temperature in K.

The SPM relaxation of a single domain magnetic nanoparticle may be observed by a technique with characteristic time (τ_s) at temperatures above the so called blocking temperature (T_B) defined by

$$T_B = KV/[k_B \ln(\tau_s/\tau_0)]. \quad (2)$$

Above the blocking temperature, the relaxation time $\tau \ll \tau_s$ ($\sim 10^{-8}$ s for ^{57}Fe Mössbauer spectroscopy) and the internal magnetic field at the nucleus is averaged out giving rise to usually a quadrupolar doublet in the Mössbauer pattern. Below the blocking temperature, $\tau \gg \tau_s$, a characteristic sextet Mössbauer pattern is observed. Near the blocking temperature when $\tau \sim \tau_s$, a partially collapsed sextet with broad lines is seen.

Mössbauer spectra recorded at room temperature of the samples with different particle sizes are shown in Figures 4, 5 and 6. The experimental data were fitted with least squares fitting programmes LGFIT2 [12] and NORMOS [13] for discrete sites and for distributions respectively. In case of discrete fitting, Lorentzian line shape is assumed in all the cases. For Zn = 0.15, all the Mössbauer spectra (Fig. 4) show a clear doublet at the central region superposed on a weak sextet. The spectra of the samples with average particle sizes 8.3 nm and 11.2 nm were fitted with one discrete doublet and one sextet. The sample with average size 12.0 nm was fitted with one doublet and two sextets. The extracted hyperfine parameters are tabulated in Table 2. The larger widths of the doublets in the present case (0.65 to 0.73 mm/s) indicate a distribution of particle size in the samples, though the spectra could not be fitted with distribution of quadrupole splittings programme. The doublets observed in all the three cases with isomer shift (IS) varying in the range 0.26–0.30 mm/s and quadrupole splitting (QS) ranging between 0.58–0.62 mm/s are attributed to

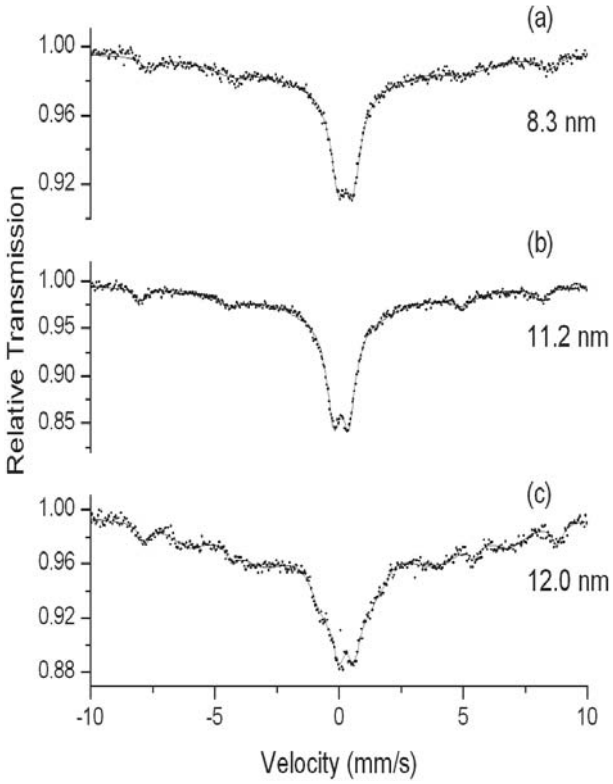

Fig. 4. Room temperature Mössbauer spectra of $Mg_{0.85}Zn_{0.15}Fe_2O_4$ having different particle sizes.

extremely small particles of ferrite in the samples undergoing SPM relaxation at room temperature where the relaxation time $\tau \ll \tau_s$. The IS values of the doublets confirm the presence of only Fe^{3+} ions in the samples [14]. The QS values of the doublets indicate substantial electric field gradient (EFG) around the ^{57}Fe nuclei. Large surface to volume ratio in nanoparticles is known to create large EFG in the ferrites though the bulk material has cubic symmetry [15]. The hyperfine parameters of the sextet (Tab. 2) for the sample with size 8.3 nm match well with that of γ-Fe_2O_3 whereas parameters for the sextet of the sample with size 11.2 nm agree well with that of α-Fe_2O_3 [16]. For the sample with size 12.0 nm, the sextet with IS = 0.36 mm/s, QS = 0.02 mm/s and internal magnetic field 40.1 T with very broad lines (FWHM $\sim$ 2.20 mm/s) is assigned to bigger particles of ferrite present in the sample for which $\tau \sim \tau_s$. The other sextet with internal magnetic field 51.6 T has been assigned to α-Fe_2O_3 [16]. The presence of γ-Fe_2O_3 / α-Fe_2O_3 phase in the present samples is most likely due to its segregation from the magnesium zinc ferrite phase during the heat treatment. The presence of a small fraction of similar oxide phases in mixed ferrite spinels had been reported by others also [10]. The maximum fraction of α-Fe_2O_3 detected in the sample heated at 720 °C was about 5%.

For Zn = 0.30, Mössbauer spectrum of the sample with average size 6.4 nm shows a clear doublet (Fig. 5a) whereas the sample with average size 11.4 nm shows a doublet (Fig. 5b) with some broadening near the shoulders.

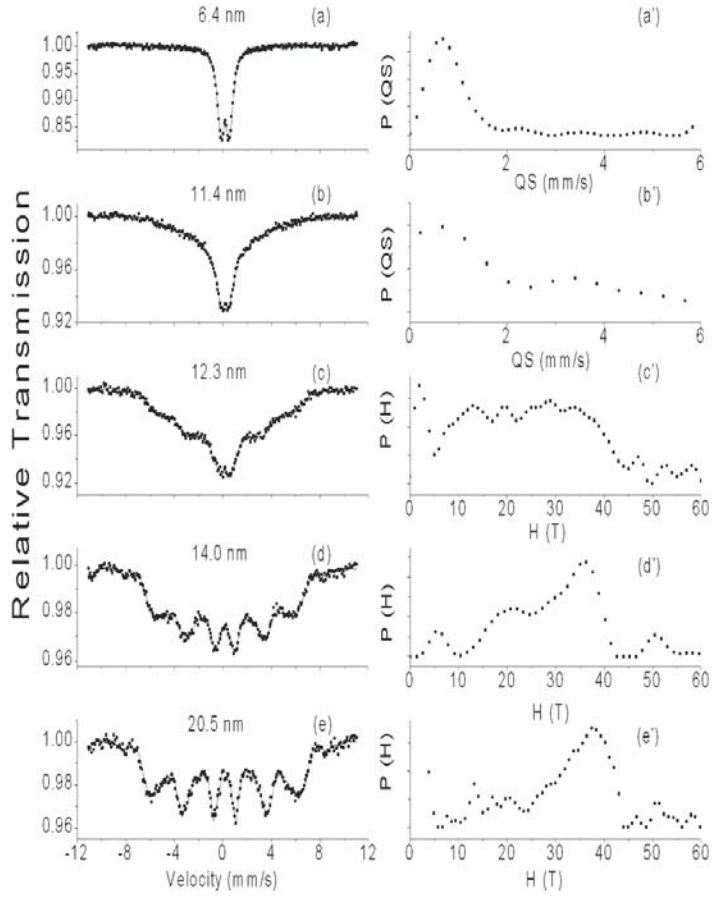

Fig. 5. Room temperature Mössbauer spectra and probability distributions of $Mg_{0.70}Zn_{0.30}Fe_2O_4$ having different particle sizes.

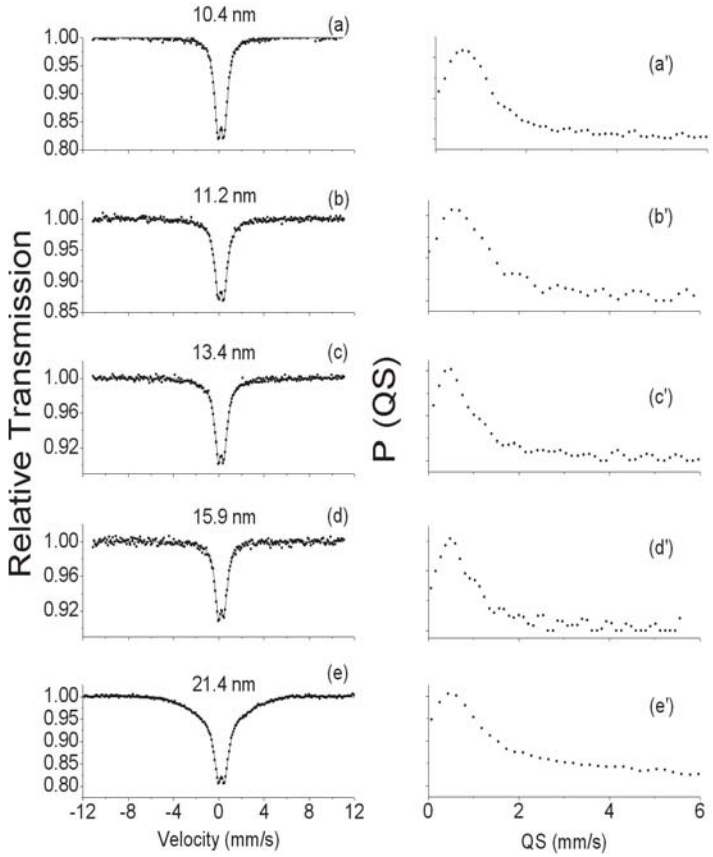

Fig. 6. Room temperature Mössbauer spectra and probability distributions of $Mg_{0.50}Zn_{0.50}Fe_2O_4$ having different particle sizes.

Table 2. Hyperfine parameters extracted from Mössbauer spectra recorded at room temperature.

Sample Composition	Particle size (nm)	Spectra fitted with	I.S.* (mm/s)	Q.S.* (mm/s)	H^*_{int} (T)
$Mg_{0.85}Zn_{0.15}Fe_2O_4$	8.3	D	0.26	0.58	-
		S	0.36	0.05	49.8
	11.2	D	0.30	0.62	-
		S	0.46	0.22	51.0
	12.0	D	0.29	0.61	-
		S1	0.48	0.20	51.6
		S2	0.36	0.02	40.1
$Mg_{0.70}Zn_{0.30}Fe_2O_4$	6.4	D	0.20	0.74	-
	11.4	D	0.29	0.42	-
	12.3	S	0.21	0.03	23.6
	14.0	S	0.17	0.04	28.4
	20.5	S	0.19	0.05	31.8
$Mg_{0.50}Zn_{0.50}Fe_2O_4$	10.4	D	0.21	0.59	-
	11.2	D	0.21	0.52	-
	13.4	D	0.20	0.50	-
	15.9	D	0.22	0.49	-
	21.4	D	0.20	0.44	-

IS = Isomer shift, QS = Quadrupole splitting (2ε), H_{int} = Internal magnetic field
D = doublet, S = Sextet
* In the case of fitting of distribution function the values tabulated are the average values.

The doublets are due to ultrafine ferrite particles undergoing SPM relaxation whereas the broadening near the shoulders are due to larger particles in the sample showing incomplete collapse of the sextet pattern. Both the spectra were fitted with distribution of quadrupole doublets and the probability distributions obtained are shown in Figures 5a′ and 5b′. The values of IS and QS extracted from the fit are shown in Table 2. The computed QS values are indicative of substantial EFG around the ^{57}Fe probe nuclei. For the sample with average size 12.3 nm a collapsing sextet (Fig. 5c) with broad lines is observed. This spectrum was fitted with distribution of hyperfine fields, the $P(H)$ vs. H obtained after the fit is shown in Figure 5c′. The broad hump observed in the region 12.0−35.0 T without a well defined peak indicates incomplete magnetic ordering in this sample consisting of particles with rather broad size distribution undergoing SPM relaxation. The average hyperfine field evaluated from the fit is 23.6 T. Mössbauer spectra of the samples with average sizes 14.0 nm and 20.5 nm (Figs. 5d and 5e respectively) were also fitted with distribution of hyperfine fields and the probability distributions are shown in Figures 5d′ and 5e′ respectively. The average hyperfine fields estimated from the fit were 28.4 T and 31.8 T respectively. The average hyperfine field is found to increase with the increase of particle size as observed by others [17].

For the samples with Zn = 0.50, clear doublets were observed with average size up to 15.9 nm which are attributed to SPM relaxation of small crystallites. The sample with average size 21.4 nm showed a little broadening near the shoulders in addition to a well-defined doublet. The shoulders are due to larger crystallites in the sample giving incomplete magnetic ordering. All the spectra (Figs. 6a–6e) could be better fitted with distribution of quadrupole doublets instead of discrete doublets, which indicates continuous variation of the electric field gradients at the ^{57}Fe nuclei, caused by distribution of particle sizes in the samples. The probability distribution curves obtained from the fit are shown in Figures 6a′–6e′. The peaks of the quadrupole splitting distributions are found to shift steadily towards the lower QS value with the increase of particle size. This is expected because particles with smaller size having larger surface to volume ratio produces larger EFG due to surface irregularities.

A comparison of Mössbauer spectra at room temperature of different samples with different zinc substitutions clearly shows that SPM properties at ambient temperature are obtained with larger crystallite size for samples with higher amount of zinc. Mössbauer spectra for all the three Zn substituted samples annealed at 500 °C were also recorded at various temperatures down to 20 K. Typical spectra obtained for the sample with Zn = 0.50 are shown in Figure 7. In all cases the intensities of the sextets were found to increase at the cost of the doublets with decrease of temperature. This confirms that the doublets observed at room temperature were due to finer crystallites of ferrites undergoing SPM relaxation. At 20 K, broad sextets were observed for all the three samples, each of these spectra was fitted with three discrete sextets. Since the samples presently studied are polycrystalline in nature and presence of any texture is unlikely, the widths and heights of the six lines of each sextet were constrained during fitting so that the area ratio of the lines (1,6): (2,5): (3,4) becomes 3:2:1. The hyperfine parameters obtained from the fit are shown in Table 3. For the sample with Zn = 0.15, the sextet with lowest IS (0.42 mm/s) is

Table 3. Hyperfine parameters extracted from Mössbauer spectra recorded at 20 K of samples heated at 500 °C.

Sample Composition	Site	IS (mm/s) (±0.02)	QS (mm/s) (±0.02)	$H_{\rm int}(T)$ (±0.2)	RA (%) (±3%)
$Mg_{0.85}Zn_{0.15}Fe_2O_4$	A	0.42	0.19	51.1	28
	B1	0.53	0.03	53.3	35
	B2	0.43	0.01	48.7	37
$Mg_{0.70}Zn_{0.30}Fe_2O_4$	A	0.41	0.14	51.3	31
	B1	0.44	0.37	51.6	30
	B2	0.45	0.02	48.6	39
$Mg_{0.50}Zn_{0.50}Fe_2O_4$	A	0.41	0.26	49.5	33
	B1	0.42	0.34	49.8	45
	B2	0.43	0.05	44.6	22

IS = Isomer shift, QS = Quadrupole splitting, RA = Relative area.

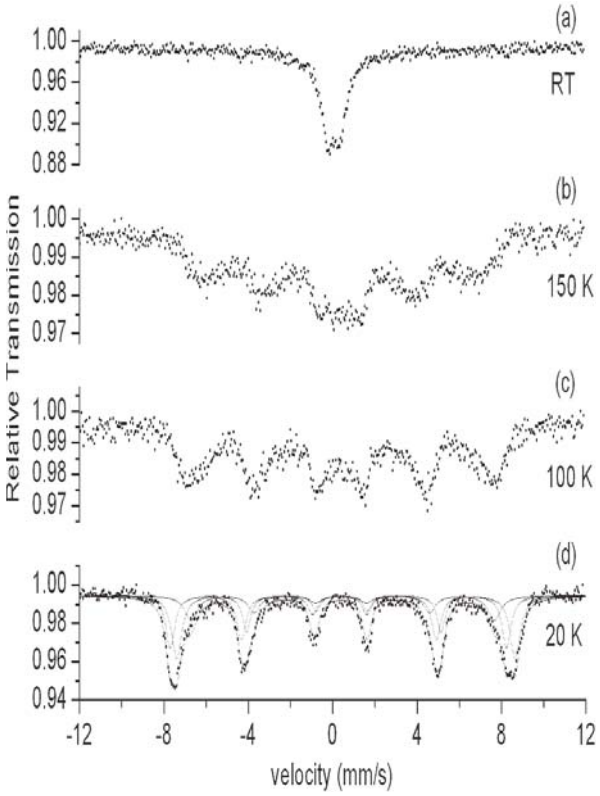

Fig. 7. Mössbauer spectra of $Mg_{0.50}Zn_{0.50}Fe_2O_4$ with particle size 13.4 nm at (a) Room Temperature (RT) (b) 150 K (c) 100 K (d) 20 K.

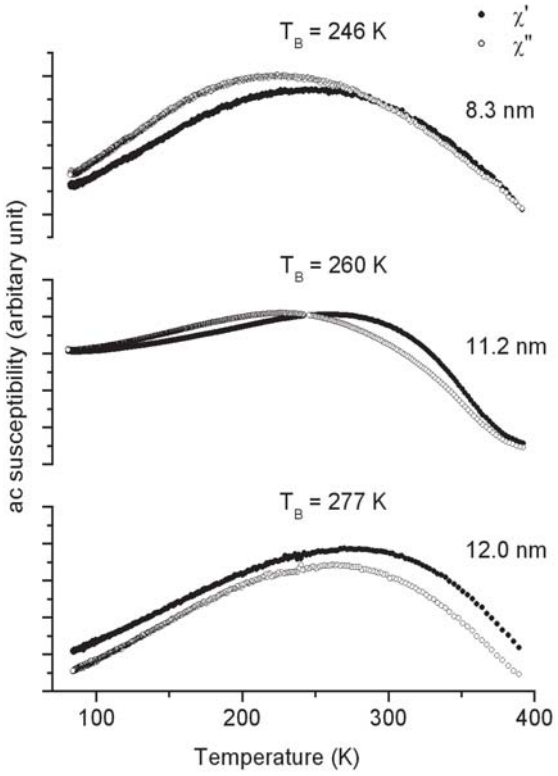

Fig. 8. AC magnetic susceptibility (χ' and χ'') of $Mg_{0.85}Zn_{0.15}Fe_2O_4$ having different particle sizes.

attributed to Fe^{3+} ions in tetrahedral (A) sites. The two other sextets with higher IS (0.53 mm/s and 0.43 mm/s respectively) are attributed to Fe^{3+} ions in two different octahedral sites (B1 and B2). As Zn^{2+} ions substitutes Fe^{3+} ions in tetrahedral sites, the Fe^{3+} ions in octahedral sites experience different local environments due to presence of Zn^{2+} ions in next nearest neighbour positions resulting in two different sets of parameters for octahedral sites. Similar assignments had been done by others also [18,19]. For the samples with Zn = 0.30 and 0.50, each of the observed Mössbauer spectra at 20 K was also assigned to one tetrahedral and two octahedral sites as has been done for the sample with Zn = 0.15 and extracted parameters are shown in Table 3. It may be noted that the internal magnetic fields at octahedral sites tends to decrease with increase of Zn concentration in A sites. The hyperfine field at the B site is known to decrease with Zn concentration in A sites as per relation $H_n = H_0(1-n\Delta H)$ where H_0 is the field at B site with no Zn ion in A site, n is the number of Zn ions in A sites and ΔH is the fractional decrease in hyperfine field [20].

3.3 AC susceptibility measurements

The thermal variations of real and imaginary part of AC susceptibilities (χ' and χ'') of all the heat-treated samples are displayed in Figures 8, 9 and 10. All observed variations clearly indicate the presence of SPM phases in

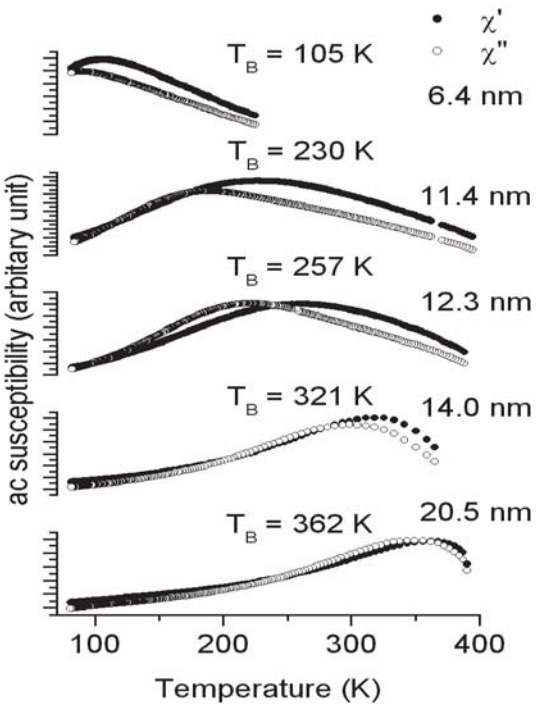

Fig. 9. AC magnetic susceptibility (χ' and χ'') of $Mg_{0.70}Zn_{0.30}Fe_2O_4$ having different particle sizes.

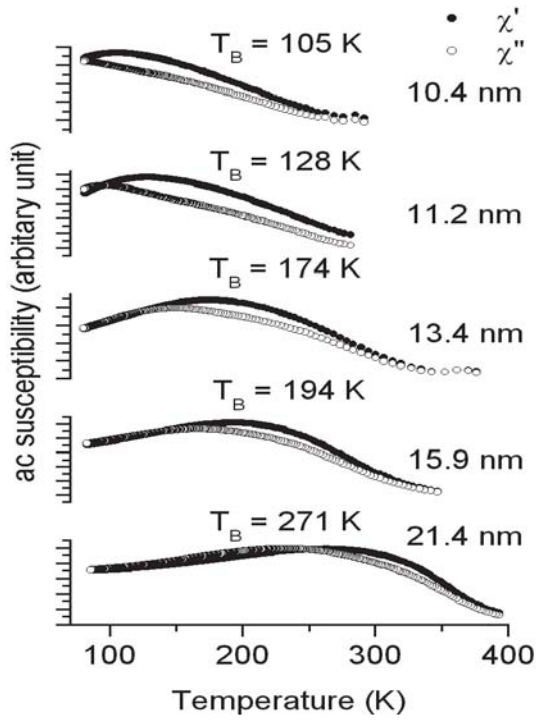

Fig. 10. AC magnetic susceptibility (χ' and χ'') of $Mg_{0.50}Zn_{0.50}Fe_2O_4$ having different particle sizes.

all the heat-treated samples. The real part of AC magnetic susceptibility increases with the decrease of temperature and shows a maximum at temperature, which is the so-called blocking temperature (T_B). Here the blocking temperature (T_B) is defined as the temperature at which the magnetic relaxation time of the particles equals to the experimental time scale of AC magnetic susceptibility measurements (τ_s) of equation (2). In the samples under present study the χ' vs. T curves gave broad maxima indicating the presence of distribution of particle sizes in the samples. The imaginary part of AC magnetic susceptibility (χ'') also has the similar nature of thermal variations like the χ' and the values of χ'' are lower compared to χ' above the blocking temperature. Here χ'' is a measure of dissipative process in the sample and its sizable observed values may be due to irreversible domain wall movement in the samples.

The blocking temperatures measured from the maxima of the real part of the AC magnetic susceptibility for all the annealed samples are presented in Table 1. Using the blocking temperatures obtained from AC magnetic susceptibility measurements and particle sizes estimated from X-ray diffraction spectra, the anisotropy energy constants were evaluated for all the annealed samples of each series using equation (2). Here τ_s is the time scale of the AC magnetic susceptibility measurements which was ∼30 ms and τ_0 has been taken as 10^{-9} s [5,11,21]. With the above parameters the condition for superparamagnetism becomes $K_AV = 17.2\ k_BT$. Here the anisotropy energy constant (K_A) is the sum of magnetocrystalline anisotropy due to dipole-dipole and/or interparticle exchange interactions together with the shape and the surface anisotropy of the nanoparticles [22]. Above the blocking temperature the particles satisfying this relation will relax during the time scale of AC magnetic susceptibility measurements. Below the blocking temperature the particles will be in a blocked state and the anisotropy energy constant can be evaluated from the relation $K_A = 17.2\ k_BT_B/V$. Figure 11 shows the variation of anisotropy energy constant with particle size for all the three Zn substituted samples. In all the samples irrespective of the size the anisotropy energy constant is always higher compared to that obtained for the bulk material [23]. For example, the value of the anisotropy energy constant in the case of bulk $MgFe_2O_4$ is 3900 J/m^3 [23] which is much lower than that obtained in the present samples. Even the lowest anisotropy energy constant value obtained in the case of $Mg_{0.50}Zn_{0.50}Fe_2O_4$ annealed at 720 °C is nearly three times more than the above bulk value. This may be due to the high contribution of surface and shape anisotropy towards K_A. The high values of anisotropy energy constant in ferrite nanoparticles were also reported by various workers [24,25]. The value of K_A is found to increase sharply with decrease of particle size (Fig. 11). This may be attributed to an increase of surface anisotropy contribution to K_A with the decrease of particle sizes. As the particle size decreases, more atoms/ions appear on the surface exhibiting higher contribution of surface anisotropy to K_A [24,26,27]. It is also observed that the value of the anisotropy energy constant for a given size decreases with the increase of Zn-content. It may be noted that the particle sizes of the samples with Zn = 0.15 annealed at 600 °C, with Zn = 0.30 annealed at 400 °C and with Zn = 0.50 annealed at 400 °C are nearly equal (∼11 nm) and the corresponding blocking

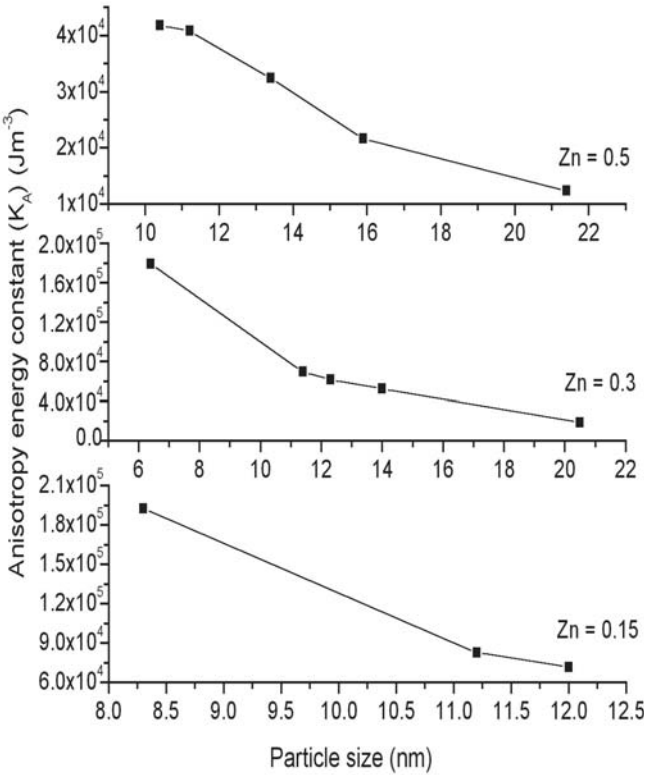

Fig. 11. Variation of anisotropy energy constant (K_A) with particle size of $Mg_{(1-x)}Zn_xFe_2O_4$ having different Zn content.

temperatures are 260 K, 230 K and 128 K respectively. Also the samples annealed at 720 °C with Zn = 0.30 and Zn = 0.50 have nearly equal particle sizes (20.5 nm and 21.4 nm respectively) and the corresponding blocking temperatures are 362 K and 271 K respectively. Thus the blocking temperature for a given particle size decreases with the increase of Zn content. For a given particle size, the lowering of T_B with the increase of Zn content may be attributed to the lowering of anisotropy energy constant (K_A) with the increase of Zn substitution.

4 Conclusions

Nanoparticles of mixed Mg-Zn–ferrite with Zn substitution up to 50% have been prepared by a simple co-precipitation method. Annealing the as prepared dried precipitate in air at various temperatures up to 720 °C results in the formation of ferrite phase with size lying in the range 6.4 nm to 21.4 nm. Increase of Zn substitution in Mg-ferrite facilitates the formation of spinel ferrite phase even at lower sintering temperature. Mössbauer results clearly show presence of SPM relaxation in all the samples. At ambient temperature, SPM properties are observed in bigger particle size in samples with higher fraction of Zn substitution. Blocking temperature measured from AC magnetic susceptibility data shows systematic fall with decrease of particle size in all the three sets of samples with various Zn substitution. Substitution of 50% Zn in Mg-ferrite results SPM relaxation at room temperature in 21.4 nm particles. The magnetic anisotropy constant increases with decrease of particle size.

References

1. C. Wang, X.M. Zhang, X.F. Qian, J. Xie, W.Z. Wang, Y.T. Qian, Mater. Res. Bull. **33**, 1747 (1998)
2. F. Bentivegna, M. Nyvlt, J. Ferre, J.P. Jamet, A. Brun, S. Visnovsky, R. Urban, J. Appl. Phys. **85**, 2270 (1999)
3. A.E. Berkowitz, R.H. Kodama, S.A. Makhlouf, F.T. Parker, F.E. Spada, E.J.Jr. McNiff, S. Foner, J. Magn. Magn. Mater. **196-197**, 591 (1999)
4. *Magnetic Properties of Fine Particles*, edited by J.L. Dormann, D. Fiorani (North-Holland, Amsterdam, 1992)
5. J. Popplewell, L. Sakhnini, J. Magn. Magn. Mater. **149**, 72 (1995)
6. K. Raj, B. Moskowitz, R. Casciari, J. Magn. Magn. Mater. **149**, 174 (1995)
7. *Scientific and Clinical Applications of Magnetic Carriers*, edited by U. Hafeli, W. Schutt, J. Teller, M. Zborowski (Plenum Press, New York, 1997)
8. V.A.M. Brabers, in: *Handbook of Magnetic Materials,* edited by K.H.J. Buschow, Vol. **8** (North Holland, Amsterdam, 1995), 189 pp.
9. Z.J. Zhang, Z.L. Wang, B.C. Chakoumakos, J.S. Yin, J. Am. Chem. Soc. **120**, 1800 (1998)
10. Qi Chen, Adam J. Rondinone, Bryan C. Chakoumakos, Z. John Zhang, J. Magn. Magn. Mater. **194**, 1 (1999)
11. L. Néel, Ann. Geophys. **5**, 99 (1949)
12. E. von. Meerwall, Comp. Phys. Commun. **9**, 117 (1975)
13. R.A. Brand, Nuclear Instr. Methods B **28**, 398 (1987)
14. G.M. Bancroft, *Mössbauer Spectroscopy: An Introduction for Inorganic Chemists and Geochemists* (McGraw-Hill Book Company (UK) Limited, 1973), Chap. 7
15. A. Hartridge, A.K. Bhattacharya, M. Sengupa, C.K. Majumdar, D. Das, S.N. Chintalapudi, J. Magn. Magn. Mater. **176**, L89 (1997)
16. N.N. Greenwood, T.C. Gibb, *Mössbauer Spectroscopy* (Chapman and Hall Ltd., London, 1971), 241 pp.
17. M. Rajendran, A.K. Bhattacharya, D. Das, S.N. Chintalapudi, C.K. Majumdar, Int. J. Mod. Phys. B **15**, 305 (2001)
18. S.A. Oliver, H.H. Hamdeh, J.C. Ho, Phys. Rev. B **60**, 3400 (1999)
19. C.N. Chinnasamy, A. Narayanasamy, N. Ponpandian, K. Chattopadhyay, H. Guerault, J.-M. Gréneche, J. Phys. C **12,** 7795 (2000)
20. Chul Sung Kim, Woo Chul Kim, Sung Yong An, Seung Wha Lee, J. Magn. Magn. Mater. **215-216**, 213 (2000)
21. R.W. Chantrell, E.P. Wohlfarth, J. Magn. Magn. Mater. **40**, 1 (1983)
22. J.L. Dormann, Rev. Phys. Appl. **16**, 275 (1981)
23. Soshin Chikazumi, *Physics of Magnetism* (Robert E. Krieger Publishing Company, 1964), 140 pp.
24. N. Moumen, M.P. Pileni, J. Phys. Chem. **100**, 1867 (1996)
25. L.D. Tung, V. Kolesnichenko, G. Caruntu, D. Caruntu, Y. Remond, V.O. Golub, C.J. O'Connor, L. Spinu, Physica B **319**, 116 (2002)
26. R.H. Kodama, A.E. Berkowitz, E.J. McNiff, S. Foner, Phys. Rev. Lett. **77**, 394 (1996)
27. M. Muroi, R. Street, P.G. McCormick, J. Amighian, Phys. Rev. B **63**, 184414 (2001)